JUN 2 2 1982

Y 3. N88:25/2544

ornl

OAK RIDGE NATIONAL LABORATORY

UNION CARBIDE

NUREG/CR-2544
ORNL/TM-7859

COMPLETED

49

ORIGINAL

Two-Phase Mass Flux Uncertainty Analysis for Thermal-Hydraulic Test Facility Instrumented Spool Pieces

N. C. J. Chen D. K. Felde

Prepared for the U.S. Nuclear Regulatory Commission
Office of Nuclear Regulatory Research
Under Interagency Agreements DOE 40-551-75 and 40-552-75

OPERATED BY
UNION CARBIDE CORPORATION
FOR THE UNITED STATES
DEPARTMENT OF ENERGY

Printed in the United States of America. Available from
National Technical Information Service
U.S. Department of Commerce
5285 Port Royal Road, Springfield, Virginia 22161

Available from

GPO Sales Program
Division of Technical Information and Document Control
U.S. Nuclear Regulatory Commission
Washington, D.C. 20555

This report was prepared as an account of work sponsored by an agency of the United States Government. Neither the United States Government nor any agency thereof, nor any of their employees, makes any warranty, express or implied, or assumes any legal liability or responsibility for the accuracy, completeness, or usefulness of any information, apparatus, product, or process disclosed, or represents that its use would not infringe privately owned rights. Reference herein to any specific commercial product, process, or service by trade name, trademark, manufacturer, or otherwise, does not necessarily constitute or imply its endorsement, recommendation, or favoring by the United States Government or any agency thereof. The views and opinions of authors expressed herein do not necessarily state or reflect those of the United States Government or any agency thereof.

NUREG/CR-2544
ORNL/TM-7859
Dist. Category AN

Contract No. W-7405-eng-26

Engineering Technology Division

TWO-PHASE MASS FLUX UNCERTAINTY ANALYSIS FOR THERMAL-HYDRAULIC TEST FACILITY INSTRUMENTED SPOOL PIECES

N. C. J. Chen D. K. Felde

Manuscript Completed – May 4, 1982
Date Published – May 1982

Prepared for the
U.S. Nuclear Regulatory Commission
Office of Nuclear Regulatory Research
Under Interagency Agreements DOE 40-551-75 and 40-552-75

NRC FIN No. B0125

Prepared by the
OAK RIDGE NATIONAL LABORATORY
Oak Ridge, Tennessee 37830
operated by
UNION CARBIDE CORPORATION
for the
DEPARTMENT OF ENERGY

I BEST DOCUMENT AVAILABLE

BLANK PAGE

CONTENTS

	Page
NOMENCLATURE	v
ABSTRACT	1
1. INTRODUCTION	1
2. SYSTEM AND INSTRUMENTATION DESCRIPTION	3
3. MODEL CALCULATIONS	10
3.1 Homogeneous Mass Flux Models	10
3.2 Kamath and Lahey Model	10
4. RESULTS AND DISCUSSION	14
4.1 Steady-State Two-Phase Flow	14
4.2 Transient Two-Phase Flow	21
5. SUMMARY AND CONCLUSIONS	33
REFERENCES	35

BEST DOCUMENT AVAILABLE

BLANK PAGE

NOMENCLATURE

A_{xs}	Effective annular flow area through the blading
C	Chord length of the blade
C_ℓ, C_v	Correlation coefficients for the liquid and vapor phases, respectively
G	Mass flux
I_{rotor}	Rotor moment of inertia
ℓ	Liquid phase
L_{jb}	Length of the journal bearing
N	Number of blades on the rotor
r	Radius measured from conduit axis
R	Effective radius of the rotor
R_b	Radius of the meter shroud
R_o	Conduit radius
R_{hi}	Bearing radius
R_s	Journal radius
R_T	Blade tip radius
S	Slip ratio
t	Time
t_b	Blade thickness
v	Vapor phase
V	Velocity
V_{cl_k}	Centerline velocity of phase k
V_k	Velocity of phase k
V_t	Turbine axial velocity
$V_{Z\ell}$	Velocity of the liquid in the axial direction
Δx	Axial distance between inlet and outlet of blade
α	Void fraction
α_{cl}	Void fraction at centerline
β	Blade angle
η_ℓ, η_v	Flow deviation factor for the liquid and vapor phases, respectively
μ	Dynamic viscosity of saturated liquid
ρ_ℓ, ρ_v	Density of saturated liquid and vapor, respectively
ω	Angular velocity of the rotor

BEST DOCUMENT AVAILABLE

TWO-PHASE MASS FLUX UNCERTAINTY ANALYSIS FOR THERMAL-HYDRAULIC TEST FACILITY INSTRUMENTED SPOOL PIECES

N. C. J. Chen D. K. Felde

ABSTRACT

An analysis of two-phase mass flux uncertainties for the Thermal-Hydraulic Test Facility (THTF) instrumented spool pieces is presented. Comparisons are made between various homogeneous mass flux models based on high-temperature and high-pressure water mass flux data from steady-state upflow film boiling tests run at the THTF. Subcooled flow at the test section inlet provides a well-defined standard for in-place evaluation of the mass flux models at the high-quality, two-phase test section outlet. Additionally, a transient two-phase turbine meter model developed by Kamath and Lahey is applied to two transient THTF tests to assess the sensitivity of the calculated mass flux to uncertainties in two-phase flow parameters and transient response as applied specifically to THTF test conditions.

---

1. INTRODUCTION

Oak Ridge National Laboratory (ORNL) has conducted a series of experiments in the Thermal-Hydraulic Test Facility (THTF) as part of the Pressurized Water Reactor (PWR) Blowdown Heat Transfer Separate Effects Program. The primary goal of the program is to produce rod bundle data that can be used to provide insight into the thermal-hydraulic behavior of light water reactor cores during hypothetical accidents. Analysis of the rod bundle test data requires measurements of mass flux, pressure, and temperature at the boundaries of the system as input for thermal-hydraulic codes. At the THTF, instrumented "spool pieces" are used to provide these measurements.

A spool piece consists of a fluid thermocouple, an absolute pressure tap, a turbine meter for measuring volumetric flow or velocity (V), a drag disk for measuring momentum flux (ρV^2), and a gamma densitometer for measuring chordal average density (ρ) of the fluid. Because the mass flux is not directly measured, combinations of these instruments must be used to determine mass flux. Homogeneous models may be used combining the turbine meter and gamma densitometer (ρV), the drag disk and the gamma densitometer ($\sqrt{\rho \cdot \rho V^2}$), and the turbine meter and drag disk ($\rho V^2/V$) to obtain mass flux. Although the uncertainties obtained using the homogeneous models should be fairly small in single-phase flow, significant uncertainties may exist in two-phase flow where effects such as slip ratio, void fraction, flow regime, and transient response affect the physical interpretation of the instrument output.

BEST DOCUMENT AVAILABLE

An analysis of mass flux uncertainties is presented based on (1) the Steady-State Upflow Film Boiling Test Series (3.07.9) run at the THTF and (2) the application of the Kamath and Lahey turbine meter evaluation model[1] to two THTF transient blowdown tests. The steady-state test series provided a good experimental method for evaluating the two-phase mass flux uncertainties over the parameter ranges of those tests. Measurement of the subcooled flow at the test section inlet provided a well-defined standard for two-phase mass flux measurements at the outlet of the test section. Previous work on evaluating mass flux models has been carried out in low-pressure steam/water and air/water facilities for THTF spool pieces.[2] The steady-state results presented in this report extend those results to in-place high-temperature and high-pressure steam/water two-phase flow conditions. The steady-state data available are limited, however, to high-quality two-phase flow conditions. The transient turbine meter evaluation model is applied to two THTF transient blowdown tests in an effort to assess the sensitivity of the calculated mass flux to uncertainties in two-phase flow parameters and transient response as applied specifically to THTF test conditions. The model is applied to the comparatively slow transient Upflow Film Boiling Test 3.06.6B (Ref. 3). The conditions of this test are fairly typical of two other upflow film boiling tests run at the THTF, 3.03.6AR (Ref. 4) and 3.08.6C (Ref. 5). The model is also applied to the faster transient test, the Double-Ended Cold Leg Break Test 3.05.5B (Ref. 6), which was a double-ended break test with a considerably faster depressurization rate than the upflow film boiling tests.

BEST DOCUMENT AVAILABLE

2. SYSTEM AND INSTRUMENTATION DESCRIPTION

A diagram of the THTF in its standard configuration is shown in Fig. 1. The test section contains an electrically heated fuel rod simulator (FRS) bundle in an 8 x 8 array typical of late generation 17 x 17 PWR bundles. The FRSs have a full 3.66-m (12-ft) heated length with a flat power profile.[7] The system is capable of operating at pressures and temperatures typical of PWRs. Transient and steady-state type tests have been run at the THTF. Transient tests are initiated by rupturing the system pressure boundaries at either the test section inlet and/or the outlet piping. Initial system pressure and test section outlet fluid temperatures are typically 15 MPa (2250 psi) and 593 K (608°F), respectively. At blowdown, the system undergoes an initial subcooled decompression followed

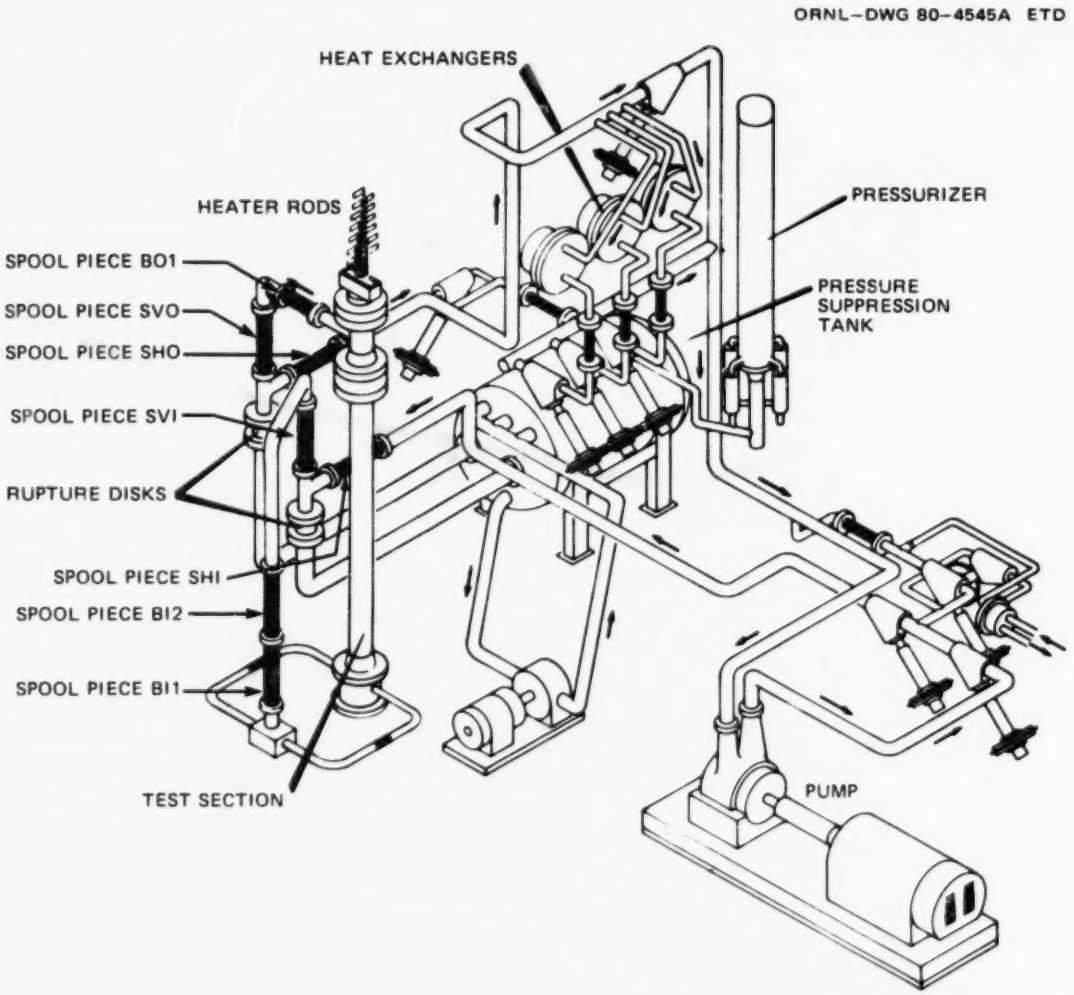

Fig. 1. THTF in standard configuration.

BEST DOCUMENT AVAILABLE

by a voiding of the system, which is controlled primarily by (1) critical flow orifices at the rupture sites and (2) power applied to the electrically heated rod bundle in the test section. Steady-state tests are operated by setting the desired inlet mass flow rate and then increasing bundle power and decreasing the system mass inventory until the desired bundle conditions are obtained.

Instrumented spool pieces are located at the inlet and outlet of the test section (Fig. 1). Diagrams of the spool pieces are shown in Figs. 2 and 3. The four original spool pieces, SHI, SVI, SHO, and SVO, are of the design shown in Fig. 2 with the densitometer positioned in the center of the spool piece. A more recent design installed at BO1, BI1, and BI2 is shown in Fig. 3. In the more recent design, the densitometer is located at the end of the spool piece. The design change was made in an attempt to eliminate effects on the densitometer measurements because of flow and flow regime disturbances caused by interference-type instruments upstream of the densitometers.[8] The densitometer end of these spool pieces is generally oriented so that the densitometer is upstream of the other instruments for the expected direction of the two-phase flow. In the standard configuration, ORNL single-beam gamma densitometers are installed on the SHI, SVI, SHO, and SVO spool pieces. The BO1, BI1, and BI2 spool pieces use Measurements, Inc., three-beam gamma densitometers. The turbine meters installed in the spool pieces are five-bladed, 3.5-in. Flow Technology turbine meters with ORNL electronics. The nominal dimension of the turbine meters is diagrammed in Fig. 4. The drag disks are Ramapo Mark V strain-gage-type drag-disk transducers with ORNL three-bladed full-flow drag-disk targets. The target as seen by the flow is shown in Fig. 5. The fluid thermocouples are Nanmac type K and project into the center of the spool-piece flow area. Pressure cells used are Precise Sensor 0- to 20.7-MPa (0- to 3000-psig) pressure transducers. For later comparison with two-phase flow results, note the individual uncertainty estimates of the spool-piece instruments in subcooled, single-phase water. These estimates[7] are listed as 2-σ values (95% confidence bands) in Table 1. For subcooled flow, the most accurate mass flux calculation is made by combining the turbine meter volumetric flow measurement and a temperature- and pressure-deduced density. Using the standard method of propagation of errors* results in a 2-σ value of 4.2% of reading for the subcooled mass flux uncertainty.

---

*The procedure referred to in the text as standard propagation of uncertainties is as follows:

Given y, if a function of a set of independent variables X_i results in $y = f(X_i)$, then the uncertainty in y, σ_y is calculated from the uncertainties in the variables X_i and σ_{X_i} using the formula

$$\sigma_y = \left[\sum_i \left(\frac{\partial f}{\partial X_i}\,\sigma_{X_i}\right)^2\right]^{1/2} .$$

BEST DOCUMENT AVAILABLE

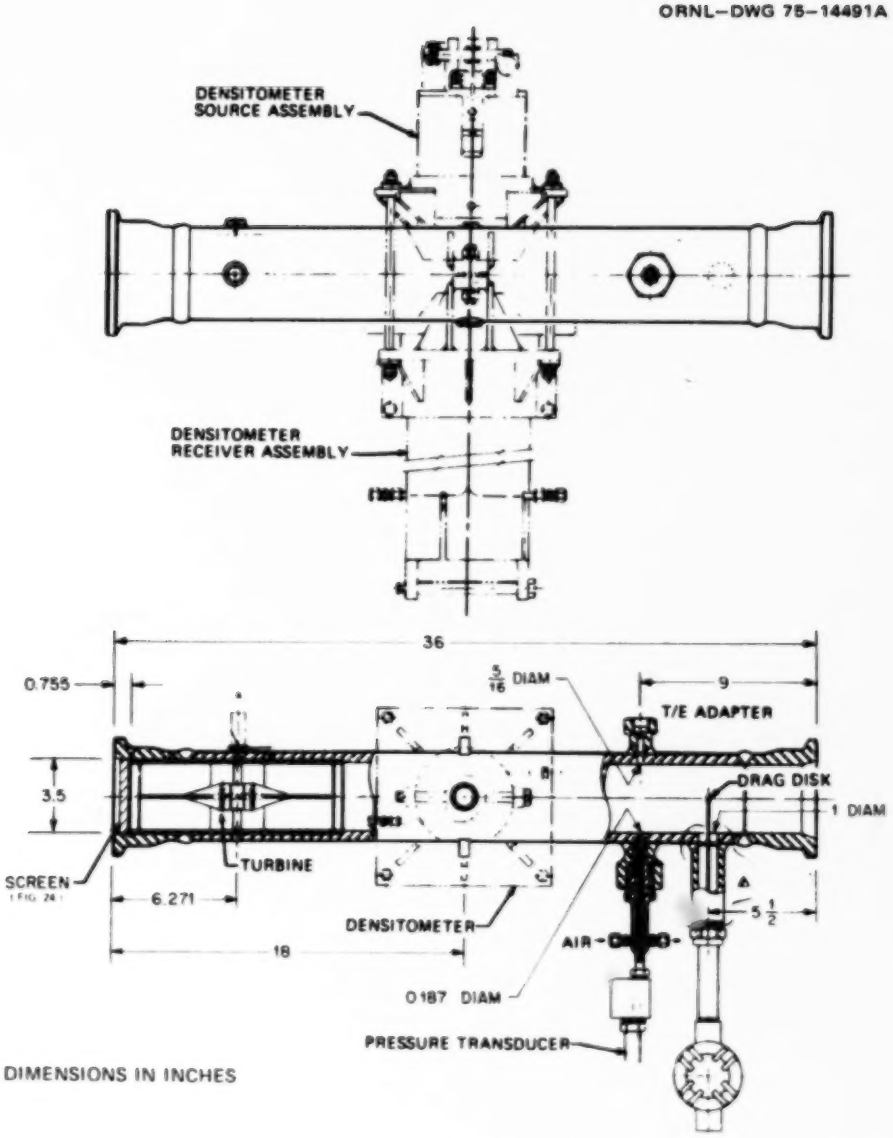

Fig. 2. Original THTF spool-piece design (spool pieces SHI, SVI, SHO, SVO).

BEST DOCUMENT AVAILABLE

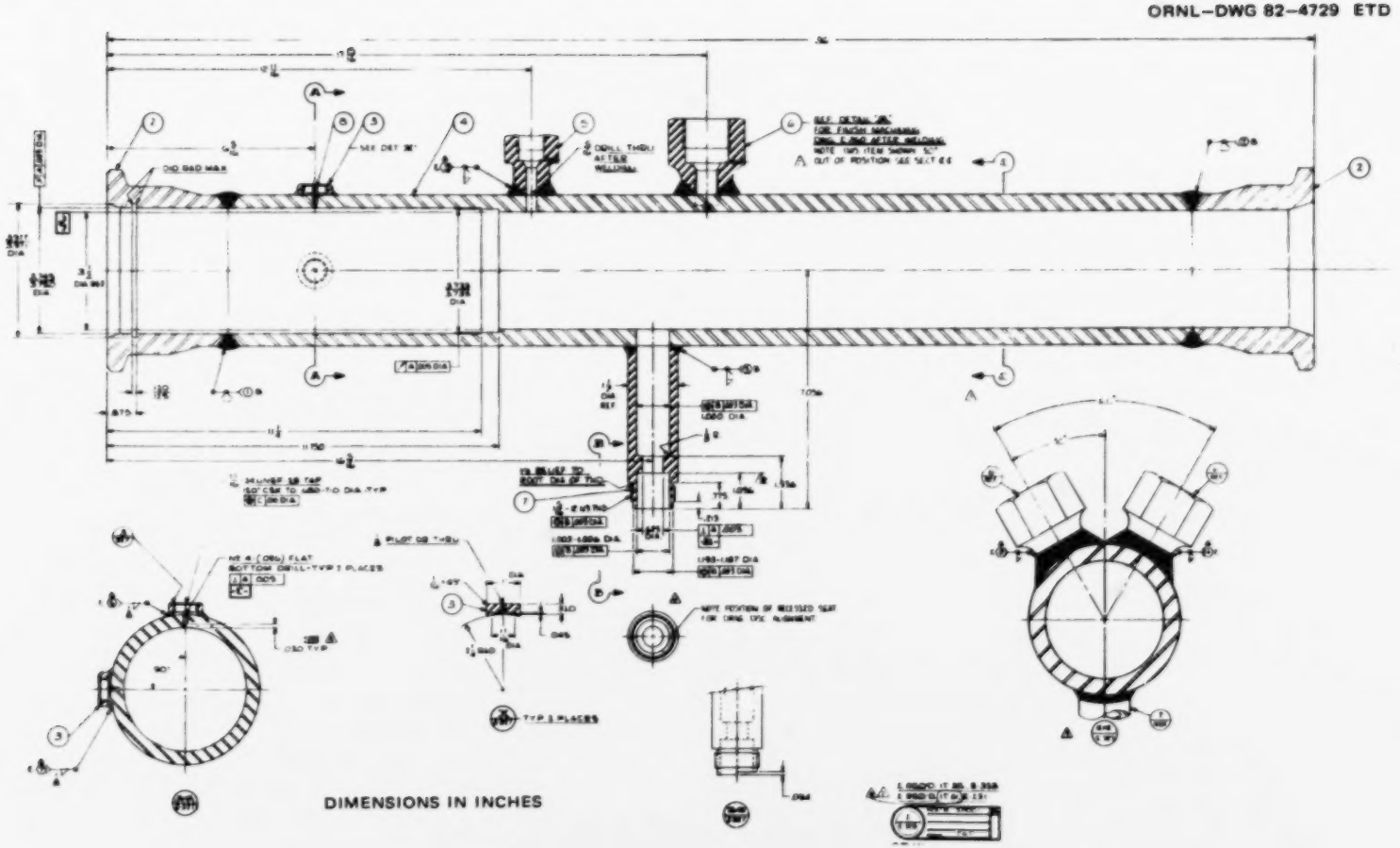

Fig. 3. Recent spool-piece design (spool pieces BI1, BI2, and BO1 in standard configuration).

BEST DOCUMENT AVAILABLE

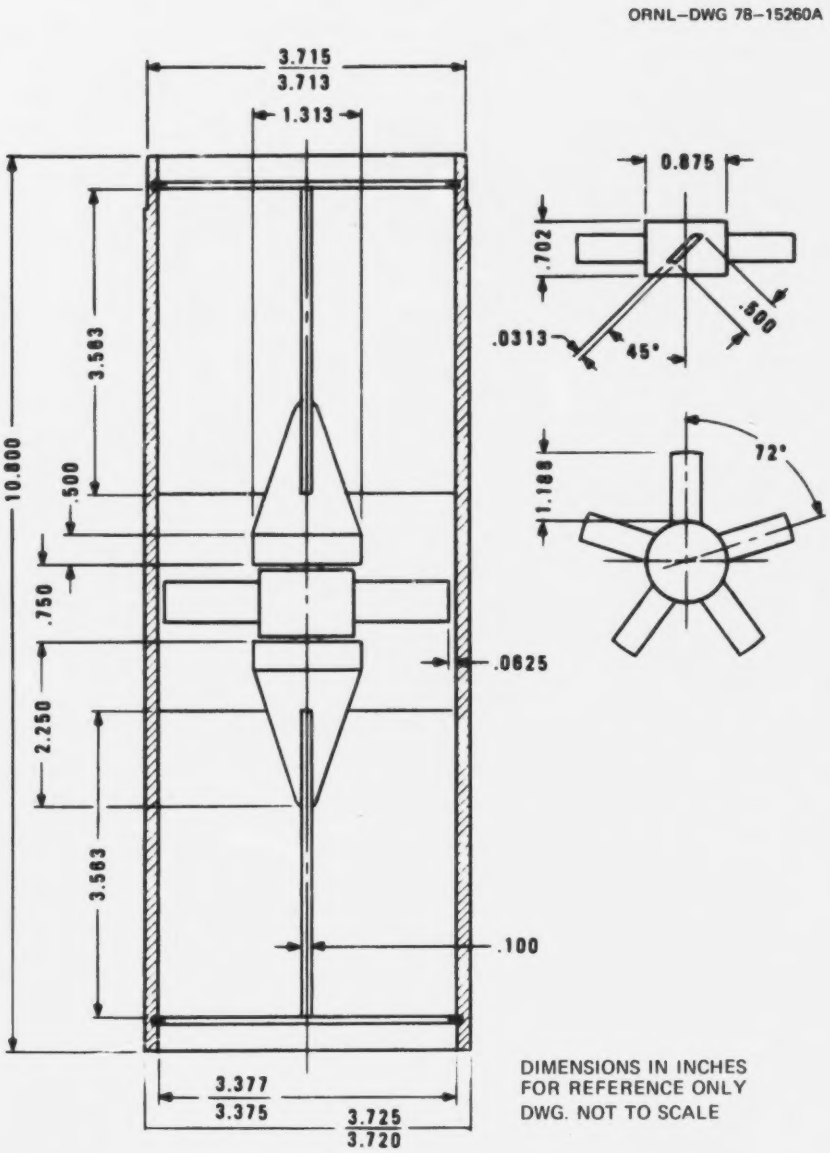

Fig. 4. Turbine flow meter assembly.

BEST DOCUMENT AVAILABLE

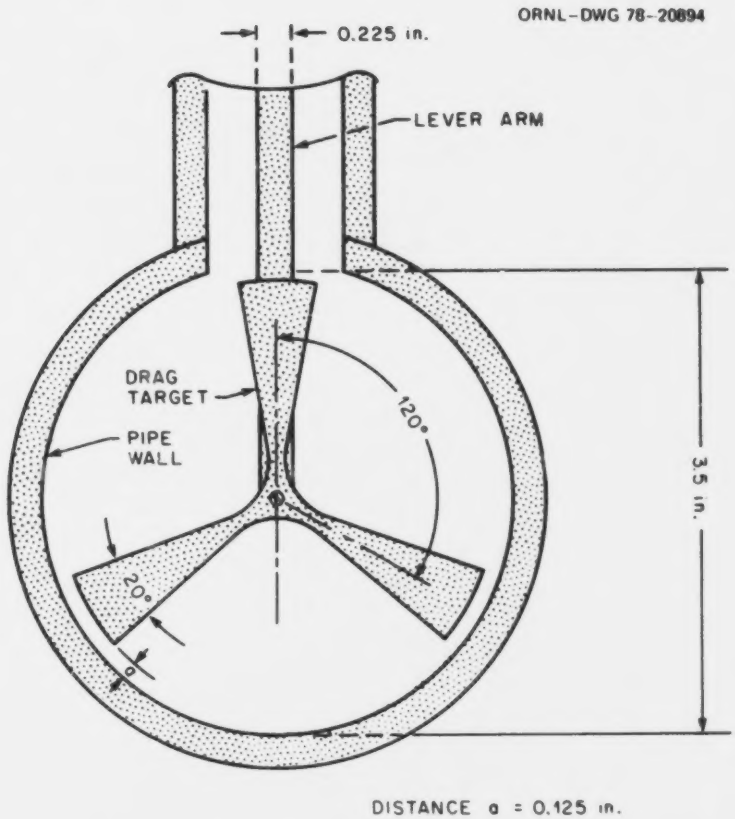

Fig. 5. Appearance of three-bladed drag target in pipe. View is looking downstream.

Table 1. Steady-state spool piece instrument uncertainties

Instrument	Uncertainty (95% confidence bands)
Precise Sensor pressure transducer, kPa (psi)	±200 (29)
Nanmac fluid thermocouple (type K), K (°F)	±3.7 ≤ 623 (6.7 ≤ 662) ±10.3 > 623 (18.5 > 662)
Flow Technology 3.5-in. turbine meter,[a] % reading	±4.1
Ramapo Mark V drag disk transducer,[a] ORNL three-bladed target, % reading	±56 for <10% full scale, ±19 for 10–100% full scale
Gamma densitometers (individual beam), kg/m³ (lb_m/ft^3)	±104 (6.5)

[a]Uncertainties based on subcooled water flow conditions.

BEST DOCUMENT AVAILABLE

As mentioned previously, a three-beam gamma densitometer is installed on spool piece B01, the first horizontal outlet spool piece. A three-region annular model[9] was used to reduce the three-beam densitometer results to a composite density suitable for use in the mass flux models. The model solves for a uniform density for each region in Fig. 6 using the density indicated by each of the three beams and the length of each beam within each region. The composite pipe density is then calculated as an area-weighted average of the three region densities. The resulting equation for the composite density is

$$\bar{\rho}_{annular} = 0.3784\rho_A + 0.5117\rho_B + 0.1099\rho_C \ , \qquad (1)$$

where ρ_A, ρ_B, and ρ_C are labeled in Fig. 6 and are the densities measured by the three beams.

Various other models may be used for combining the three chordal density measurements, such as the stratified model described in Ref. 8. However, air/water studies[8] indicate that little difference (~5%) is observed between the two models.

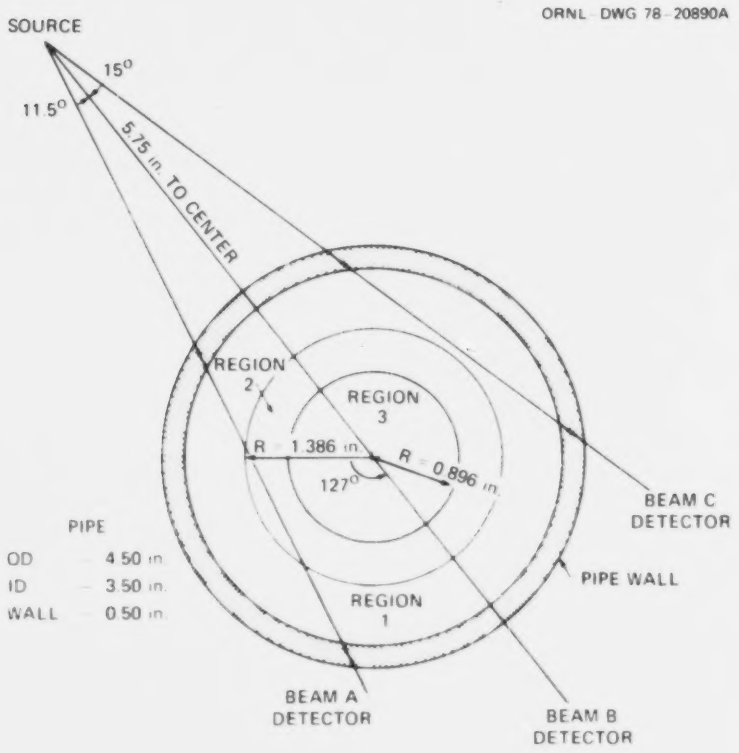

Fig. 6. Diagram showing uniform density regions used in annular model for reduction of three-beam densitometer data.

BEST DOCUMENT AVAILABLE

3. MODEL CALCULATIONS

3.1 Homogeneous Mass Flux Models

As mentioned earlier, the homogeneous mass flux models are simply combinations of measured values of pipe-averaged velocity, momentum flux, and density. The three models are indicated below:

$$G(\text{turbine meter/densitometer}) = \rho V \ , \tag{2}$$

$$G(\text{turbine meter/drag disk}) = (\rho V^2/V) \ , \tag{3}$$

$$G(\text{drag disk/densitometer}) = (\rho \cdot \rho V^2)^{1/2} \ , \tag{4}$$

where

G = mass flux, $kg/m^2 \cdot s$ ($lb_m/ft^2 \cdot s$) ,

ρ = density, kg/m^3 (lb_m/ft^3) ,

V = velocity, m/s (ft/s) .

These mass flux models are incorporated into the mass flux code AMICON (Ref. 10), which operates on the transient instrument data at each time step of a data scan. Where conditions permit, in subcooled or superheated flow, the density for the models is deduced from water properties based on temperature and pressure measurements and replaces the densitometer-measured density. The uncertainty in density determined in this manner is significantly less than the uncertainty inherent in the densitometer-measured density. Logic in AMICON and water properties codes determine whether a temperature- and pressure-deduced density or a densitometer-measured density is appropriate (based on a comparison of measurements by these same instruments). For saturated-flow conditions, the logic also prevents use of a densitometer-measured density that is less than the saturated vapor density (within uncertainty bands) for the measured temperature and pressure in the spool piece. For high-quality mass flows, this effectively reduces uncertainties on the low side of the density measurements.

3.2 Kamath and Lahey Model

The turbine flowmeter model developed by Kamath and Lahey will be briefly described in this section, along with its assumptions and limitations. The computer solution technique and input parameters are also discussed.

The turbine flowmeter dynamic equation was derived from the principle of angular momentum conservation. The equation accounts for (1) effects

BEST DOCUMENT AVAILABLE

of nonuniformity of velocity and void profiles in conduit, (2) imperfect guidance of the fluid by the rotor blades, (3) rotor inertia, (4) slip ratio, (5) bearing friction, and (6) windage losses. A detailed derivation of the equation of motion is presented in Ref. 1. The resulting equation of motion is shown below:

$$\frac{d\langle V_{Z\ell}\rangle}{dt} = \langle |V_{Z\ell}| \rangle \frac{V_t}{(\Delta x)} - \langle V_{Z\ell}\rangle \left[\frac{R_1}{(S + R_1)\rho_\ell} \frac{d\rho_\ell}{dt} \right.$$

$$\left. + \frac{S}{(S + R_1)\rho_v} \frac{d\rho_v}{dt} + \frac{S - R_2}{S + R_1} \frac{1}{\langle\alpha\rangle} \frac{d\langle\alpha\rangle}{dt} + \frac{1}{(S + R_1)} \frac{dS}{dt} \right]$$

$$- \frac{C_\ell R_1 + C_v S^2}{(S + R_1)(\Delta x)} \langle V_{Z\ell} \times |V_{Z\ell}| \rangle + V_t \left[\frac{R_1}{(S + R_1)} \frac{1}{\rho_\ell} \frac{d\rho_\ell}{dt} \right.$$

$$\left. + \frac{S}{(S + R_1)} \frac{1}{\rho_v} \frac{d\rho_v}{dt} + \frac{1 - R_2}{S + R_1} \frac{1}{\langle\alpha\rangle} \frac{d\langle\alpha\rangle}{dt} \right] + \frac{dV_t}{dt} \left[\frac{1 + R_1}{S + R_2} \right.$$

$$\left. + \frac{I_{rotor}(1 + \eta_v)}{(S + R_1)R^2 A_{xs}(\Delta x)\rho_v\langle\alpha\rangle} \right] + \frac{\mu^{0.43}\rho_\ell^{0.57}|\omega|^{0.57}\,\omega(1 + \eta_v)}{(S + R_1)RA_{xs}(\Delta x)\tan\beta\rho_v\langle\alpha\rangle}$$

$$\times \left[0.039(Ct_b N)R_T^{2.57}\,(R_b - R_T)^{-0.43} + 0.078(L_{jb}R_S^{3.57})\right.$$

$$\left. \times\, (R_{h_1} - R_S)^{-0.43}\right] . \quad (5)$$

The angular brackets in the equation are cross-sectional average operators. The variables R_1, R_2, and V_t are defined by

$$R_1 = R_2 \frac{(1 - \alpha)}{\alpha} , \quad (6)$$

$$R_2 = \frac{\rho_\ell}{\rho_v} \frac{(1 + \eta_v)}{(1 + \eta_\ell)} , \quad (7)$$

$$V_t = \frac{\omega R}{\tan\beta} . \quad (8)$$

BEST DOCUMENT AVAILABLE

The variable definitions are listed in the nomenclature. Equation (5), a classical separated-flow equation, is derived for arbitrary void fraction and velocity profiles by assuming that cross-sectional average products may be separated into products of averages using correlation coefficients. In this case, the correlation coefficients C_ℓ and C_v relate commonly measured values such as average cross-sectional void fraction (average density) and average cross-sectional velocity to void fraction and velocity profile weighted averages of the separate-phase momentum flux. The correlation coefficients appearing in Eq. (5) are defined as

$$C_\ell = \frac{\langle (1 - \alpha)\ V_\ell^2 \rangle}{\langle 1 - \alpha \rangle\ \langle V_\ell \rangle^2} \tag{9}$$

and

$$C_v = \frac{\langle \alpha V_v^2 \rangle}{\langle \alpha \rangle\ \langle V_v \rangle^2} \tag{10}$$

for the liquid and vapor phases, respectively. These coefficients relate the net momentum flux to the mean velocities of the components and may assume different values for various flow regimes. The parameters are, in effect, adjustments to homogeneous model inputs for nonhomogeneous flow effects. The magnitude of the effect of these coefficients on the mass flux as applied to THTF test conditions will be discussed later.

The dynamic equation is solved using an IBM subroutine, Continuous System Modeling Program III (CSMP III), designed to solve a system of first-order differential equations with initial values.[11] The subroutine is limited, however, to input parameters with analytical forms.

The main input to the program includes the turbine meter geometry, transient pressure, two-phase cross-sectional average density, and the turbine meter counting rate, which is proportional to the blade angular velocity. Discrete data are recorded during the transients by a data acquisition system at 10-ms intervals. Analytical forms of the data were produced from the discrete data for input to the CSMP III program.

The equation for steady-state flow in a conduit may be obtained by setting all time derivatives to zero in Eq. (5). For steady-state model comparison, note that the steady-state model reduces to the Rouhani model[12] under certain simplifying assumptions. If (1) the correlation coefficient between void fraction and velocity profiles is unity (i.e., $C_\ell = C_v = 1$), (2) the guidance of the fluid by the rotor blade is perfect ($\eta_\ell = \eta_v = 0$), and (3) the drag torque is assumed negligible, then Eq.(5) may be further reduced to the Rouhani model equation,

$$\langle \alpha \rangle\ \rho_v\ \langle |V_v| \rangle\ [\langle V_v \rangle - V_t] = \langle 1 - \alpha \rangle\ \rho_\ell\ \langle |V_\ell| \rangle\ [V_t - \langle V_\ell \rangle]\ , \tag{11}$$

BEST DOCUMENT AVAILABLE

which assumes a momentum balance between two phases on the turbine blades. Values of η_ℓ and η_v for the transient results that follow are assumed to be 0.2, a typical value for single-phase flow reported in Ref. 1. Parametric studies by Kamath and Lahey indicate very little difference between the 0.0 and 0.2 assumed values for η_ℓ and η_v. For the purposes of this analysis, a steady-state and transient model reference case is defined that assumes typical parameter values of $S = 1$, $C_\ell = 0.99$, $C_v = 1.06$, $\eta_\ell = 0.2$, and $\eta_v = 0.2$. Values of C_ℓ and C_v are from Ref. 1 where power law velocity and void profiles were assumed:

$$V_k = V_{cl_k} (1 - r/R_o)^{1/n} \quad \text{for } n = 2\text{–}7 , \tag{12}$$

and

$$\alpha = \alpha_{cl} (1 - r/R_o)^{1/m} \quad \text{for } m = 2\text{–}7 . \tag{13}$$

BEST DOCUMENT AVAILABLE

4. RESULTS AND DISCUSSION

4.1 Steady-State Two-Phase Flow

A limited amount of steady-state two-phase mass flux uncertainty data over an equilibrium quality range of ~0.8 to 1.4 are available from the Steady-State Upflow Film Boiling Test Series (3.07.9) run at the THTF. The test series was run primarily to obtain heat transfer data for film boiling in upflow over pressure and mass flux ranges of interest for reactor safety studies. The spool pieces of interest for this analysis are at the test section outlet where two-phase dispersed flow is expected for the high equilibrium quality conditions. Steady-state subcooled flow at the test section inlet provides a reference standard for estimating the two-phase mass flux uncertainty at the test section outlet spool pieces. The various homogeneous mass flux models described earlier are compared with each other as a function of pressure, equilibrium quality, and inlet mass flux. The data were obtained over a range of parameters indicated below:

1. pressure: 5.5–13.8 MPa (800–2000 psi),
2. mass flux: 195–830 kg/m²·s (40–170 $lb_m/ft^2 \cdot s$), and
3. equilibrium quality: 0.8–1.4.

Note in looking at the comparisons that the tests were not parametric in the sense that only one parameter was varied at a time. The same data set is used for comparisons as a function of pressure, equilibrium quality, and inlet mass flux. Each of the homogeneous model mass flux data points shown in the figures is an average of over 200 AMICON calculated mass flux data points taken at 0.05-s intervals over a 10-s scan period. Results from a steady-state version of the Kamath and Lahey model are also presented for comparison. This comparison is useful in providing confidence limits on the transient model as applied specifically to the THTF instruments.

For convenience, the various mass flux models are abbreviated as shown below:

1. turbine meter/single-beam densitometer = TBM-GAM,
2. turbine meter/three-beam densitometer = TBM-GAM3,
3. drag disk/single-beam densitometer = DD-GAM,
4. drag disk/three-beam densitometer = DD-GAM3,
5. turbine meter/drag disk = TBM-DD, and
6. Kamath and Lahey = K and L.

The steady-state model results are plotted as the ratio of the model mass flux to the reference inlet mass flux, G(MODEL)/G(REFERENCE), where perfect agreement is at 1.0. Note, as mentioned earlier, that the reference subcooled inlet mass flux has 95% confidence bands of ±4.2% (from a turbine meter measured velocity and a temperature- and pressure-deduced density).

The mass flux model DD-GAM3, TBM-DD, TBM-GAM3, and K and L are compared in Figs. 7–9 as functions of pressure, equilibrium quality, and

BEST DOCUMENT AVAILABLE

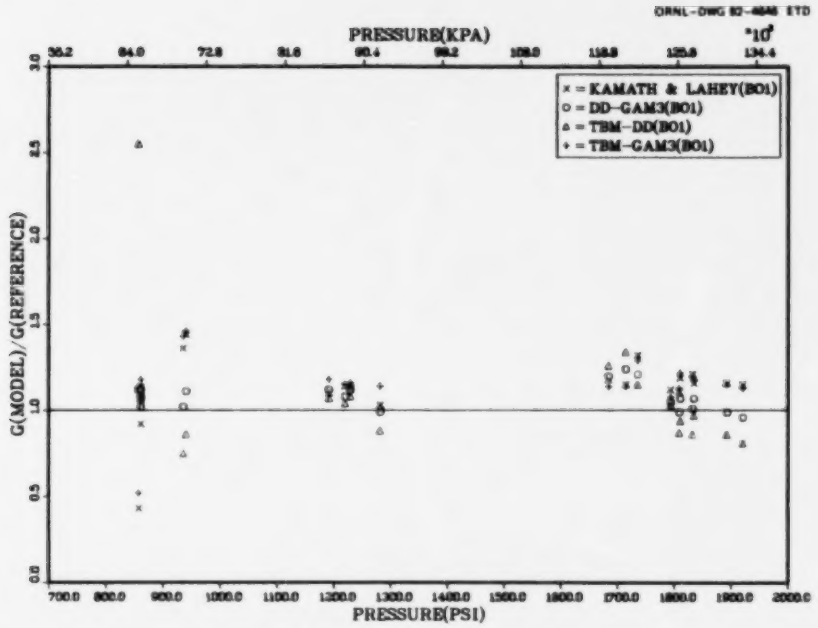

Fig. 7. Comparison of mass flux models vs pressure at B01 spool piece.

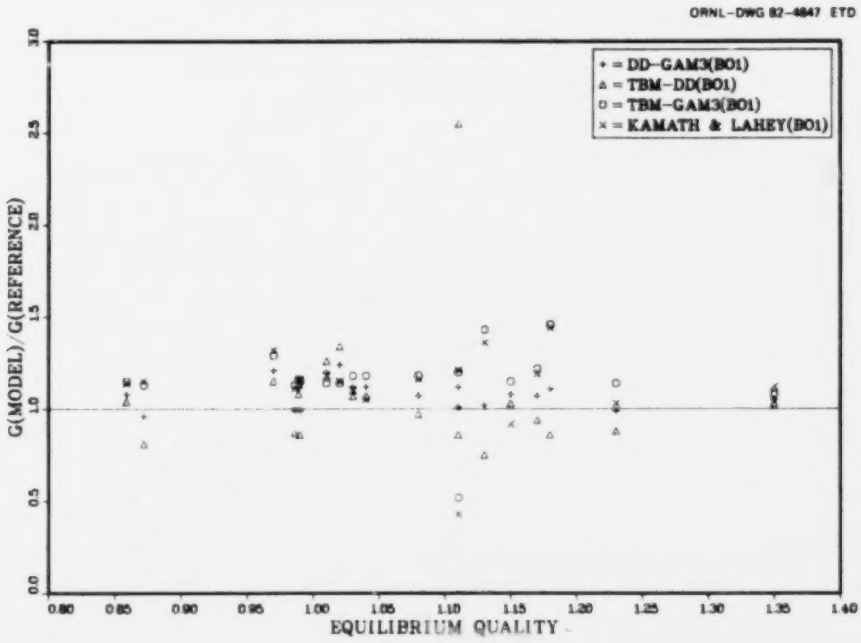

Fig. 8. Comparison of mass flux models vs equilibrium quality at B01 spool piece.

BEST DOCUMENT AVAILABLE

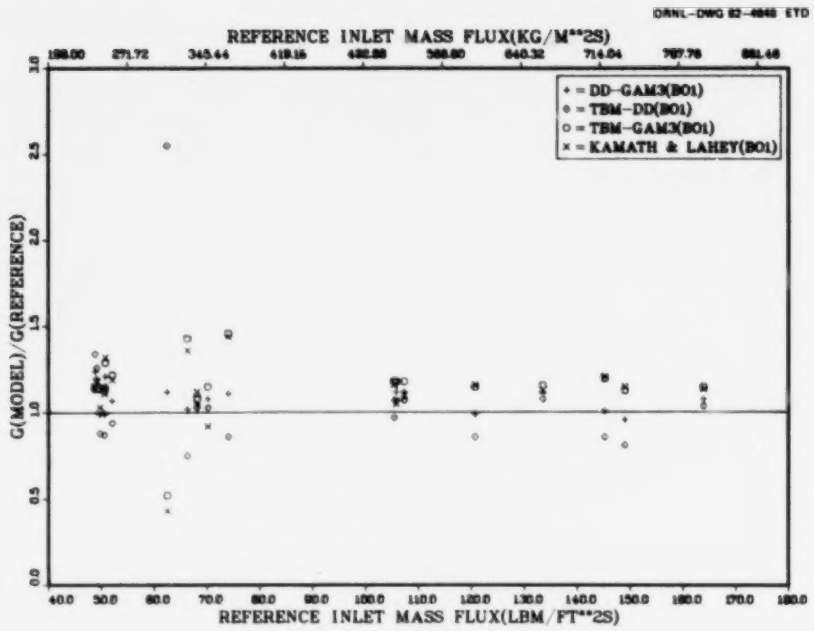

Fig. 9. Comparison of mass flux models vs inlet mass flux at B01 spool piece.

inlet mass flux, respectively. The results are from the first horizontal bundle outlet spool piece (B01). All of the models generally fall within 95% confidence bands of ±50%. Data scatter increases somewhat for lower pressures and mass flux. The DD-GAM3 and TBM-DD models show somewhat smaller uncertainty bands (approximately ±30%) than the TBM-GAM3 and K and L models. The TBM-GAM3 and the K and L model agree quite closely over the range of test parameters.

The three-beam densitometer was used in the previous comparisons; use of a single-beam densitometer in the models results in significantly higher uncertainties (Figs. 10 and 11). Comparisons are made between the TBM-GAM and the TBM-GAM3 models in Fig. 10 and the DD-GAM and DD-GAM3 models in Fig. 11 at the B01 spool piece. The single-beam model uses the center beam measurement of the three-beam densitometer to provide the comparison. The only essential difference between this beam and the standard single-beam densitometers located on the other horizontal spool pieces is the orientation of the beam. The optimum orientation for a single-beam densitometer positioned on a horizontal spool piece is in the vertical plane. The orientation of the center beam of the three-beam densitometer is at 37° from the vertical plane (see Fig. 6). For the high-quality dispersed flow believed to exist for these tests, however, the orientation is not expected to cause significant model differences (i.e., this would not be the case for stratified flow). Uncertainty bands increase from approximately ±50% for the TBM-GAM3 model to ±80% for the TBM-GAM model. Uncertainty bands for the DD-GAM model are ~10% higher than for the DD-GAM3 model. An assumption that the model for reducing the three-beam data to a

BEST DOCUMENT AVAILABLE

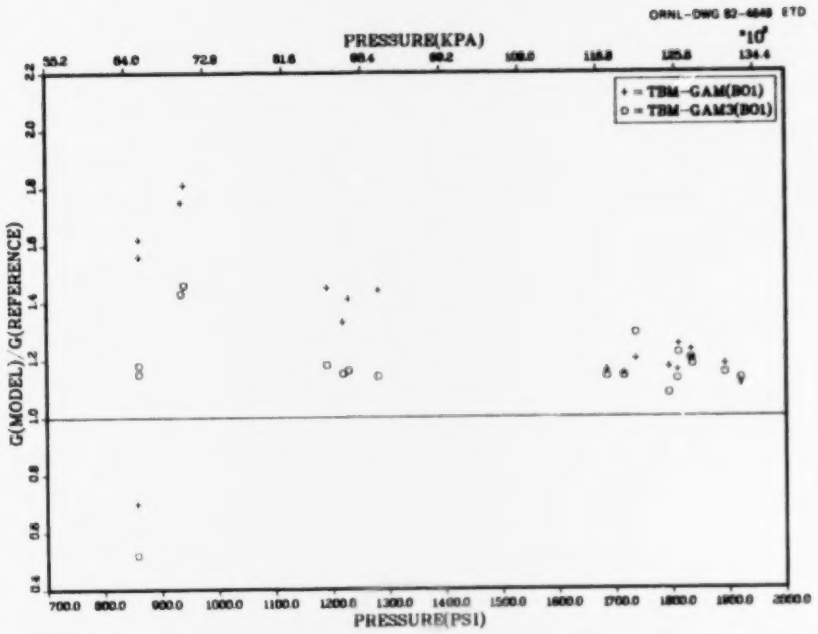

Fig. 10. Comparison of turbine meter/densitometer models using single-beam and three-beam densitometers at B01 spool piece.

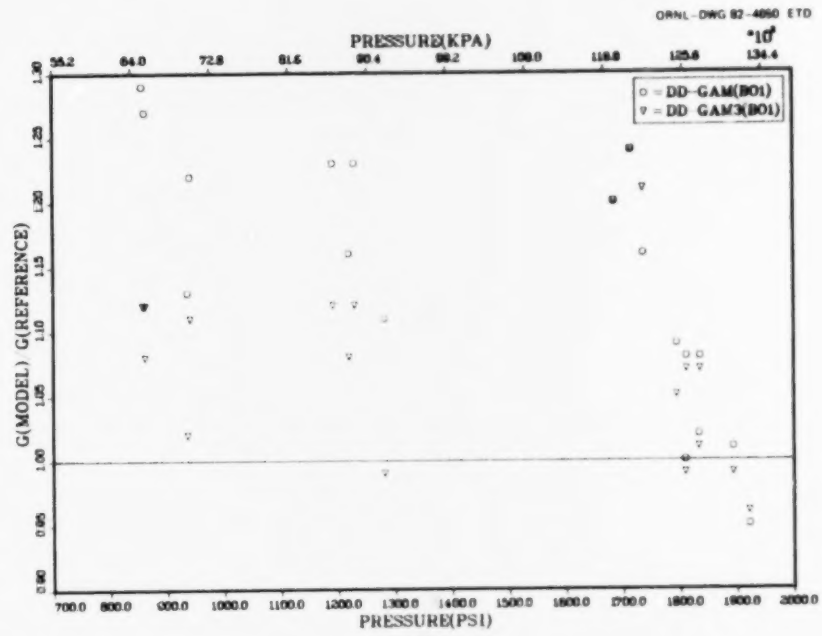

Fig. 11. Comparison of drag disk/densitometer models using single-beam and three-beam densitometers at B01 spool piece.

BEST DOCUMENT AVAILABLE

composite density is the primary factor in reducing the mass flux uncertainties may be misleading. The reduction in measurement uncertainties observed under the high-quality flow condition possibly is simply the result of improved statistics (i.e., three measurements of the average pipe density vs one measurement for a single-beam densitometer) rather than a result of the three-beam densitometer illuminating more of the pipe cross section and measuring variations in density over the pipe cross section. In any case, use of the three-beam densitometer does considerably improve the mass flux uncertainties.

Mass flux model comparisons were also made at the other two outlet spool pieces, SVO and SHO. Spool piece SVO is a vertical spool piece with downflow and follows the BO1 spool piece in the normal flow direction. Spool piece SHO is a horizontal spool piece that follows SVO. As mentioned earlier, flow conditions at the upper end and outlet of the test section were primarily dispersed flow with considerable thermal nonequilibrium for many of the data points. As the flow moves downstream from the test section outlet, equilibrium is eventually reached as the liquid droplets evaporate. For equilibrium qualities >1.0, single-phase superheated steam conditions should eventually exist. The three homogeneous models are compared vs equilibrium quality for the SVO spool piece in Fig. 12. Uncertainty bands for the DD-GAM model (~70%) and for the TBM-DD model (~140%) are significantly higher than those observed at the horizontal BO1 spool piece. Note that the significantly higher uncertainties for the models incorporating drag-disk measurements in the vertical spool

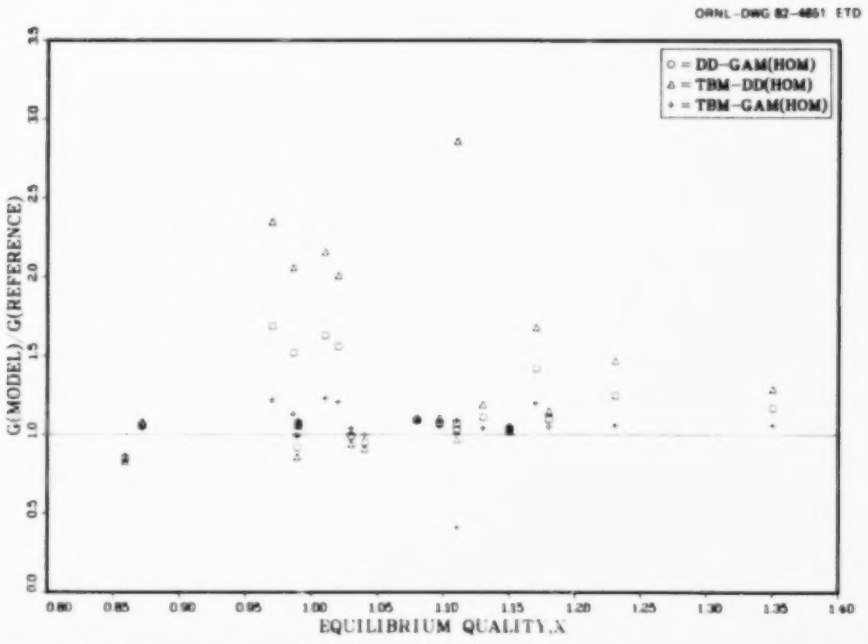

Fig. 12. Comparison of mass flux models vs equilibrium quality at SVO spool piece.

BEST DOCUMENT AVAILABLE

piece SVO as compared with the uncertainties observed for the same models in the horizontal BO1 spool piece are not necessarily the result of flow regime or orientation effects. From the standpoint of previous operating experience, the drag disks are the least reliable of the spool piece instruments in terms of repeatability and consistency of instrument response to conditions in the fluid. A trend of decreasing uncertainty at higher equilibrium qualities is observed in the data at the SVO spool piece. This may indicate that (1) the flow is approaching equilibrium conditions and (2) the flow is essentially single-phase superheated steam. Figure 13 shows the same comparisons for the SHO spool piece. The flow appears to reach equilibrium at this spool piece. The uncertainties for all of the models at the SHO spool piece have approximately the uncertainty bands expected for single-phase flow (i.e., the 2-σ uncertainty bands for the drag-disk instruments in subcooled flow are ±19% of reading over 10–100% of range; as a result, models using this instrument would have 2-σ uncertainty bands >19%).

The validity of applying the steady-state uncertainty results obtained in the THTF to other quality ranges and flow regimes is somewhat questionable. Some indication of the expected trends in the mass flux model uncertainties with quality may be obtained, however, from air/water experiments conducted with similar spool pieces.[3] Results are taken from Ref. 2 and shown in Figs. 14–16 for the three homogeneous models TBM-GAM3, DD-GAM3, and TBM-DD. The results are for qualities up to ~50%. The trends for the TBM-GAM3 and DD-GAM3 models show increasing overprediction by the

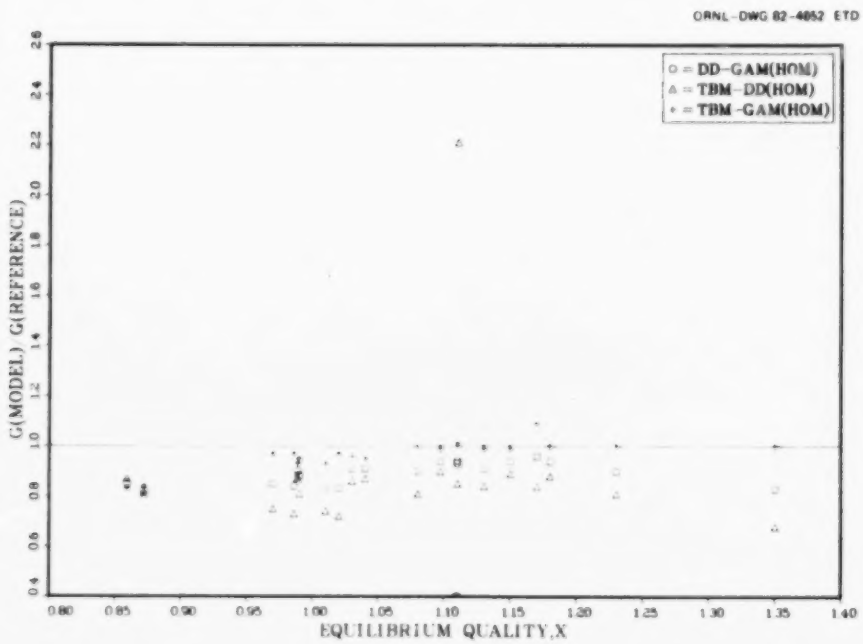

Fig. 13. Comparison of mass flux models vs equilibrium quality at SHO spool piece.

BEST DOCUMENT AVAILABLE

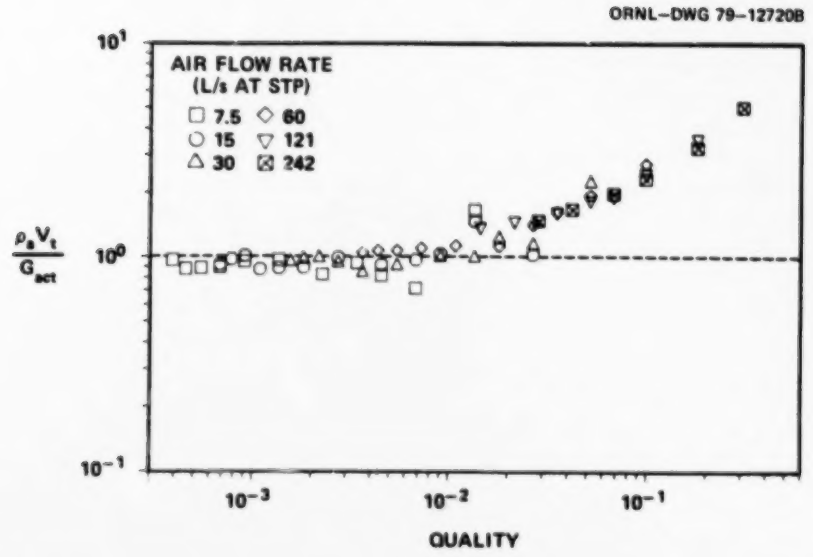

Fig. 14. Ratio of mass flux determined using densitometer and turbine meter to actual mass flux in horizontal two-phase flow (Air/Water Test Facility).

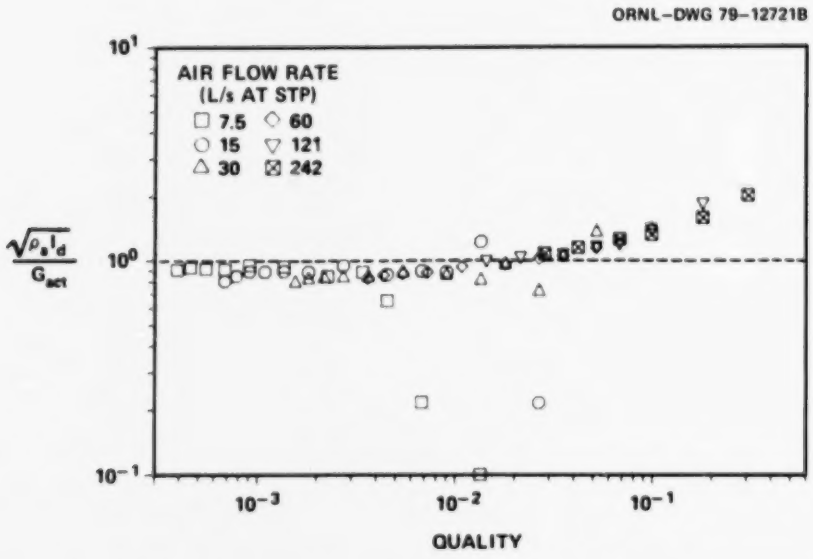

Fig. 15. Ratio of mass flux determined using densitometer and drag flowmeter to actual mass flux in horizontal two-phase flow (Air/Water Test Facility).

BEST DOCUMENT AVAILABLE

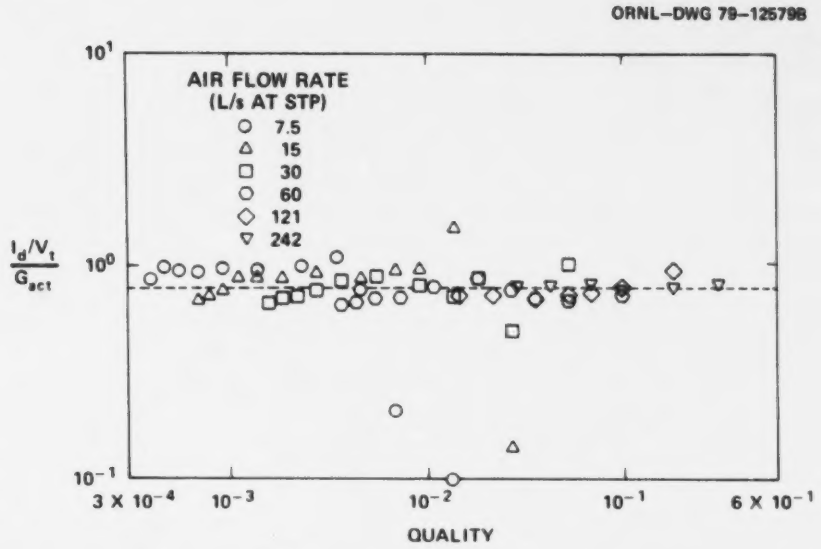

Fig. 16. Ratio of mass flux determined using turbine meter and drag flowmeter to actual mass flux in horizontal two-phase flow (Air/Water Test Facility).

models with increasing quality. The TBM-DD model does not show any significant trends over the range of quality shown. If these results can be extended to high-pressure and high-temperature steam/water data, then the inference is that the high-quality mass flux uncertainty results obtained in the THTF should apply conservatively over lower quality ranges (especially for the TBM-GAM3 and DD-GAM3 models). This assumption has not been validated experimentally, however, and should be used with caution because the quality ranges of the air/water test results do not include the higher quality ranges of the THTF tests. Possible flow regime changes at the higher qualities could disrupt the observed trends.

4.2 Transient Two-Phase Flow

The application of the K and L transient two-phase turbine meter model to THTF test data is made in an attempt to assess the effects of slip, void fraction, flow regime, and transient response on the physical interpretation of the instrument output. Verification of the model in transient two-phase flow is not possible for the THTF because of the nature of the tests and system. The intent rather is to look at effects that are not accounted for in the simpler homogeneous flow models as they apply to THTF test conditions.

As stated earlier, the model incorporates the effects of rotor inertia, velocity and void profiles in the conduit, slip ratio, imperfect guidance of the fluid by the rotor blades, bearing friction, and windage losses. Of these parameters, the effects of the velocity profiles of the

BEST DOCUMENT AVAILABLE

liquid phase, void profiles, rotor inertia, and slip ratio were found to be the most significant for the transients of interest.

Transient model solutions were obtained from data from portions of two transient tests run at the THTF. Because reference mass flux information is not available under the transient conditions, the model results are compared with a homogeneous mass flux model (TBM-GAM3). The homogeneous mass flux is obtained from the product of the average mixture density as measured by the three-beam gamma densitometer and the average velocity as deduced from the volumetric flow measurement of the turbine meter (based on subcooled water calibration factors). Comparing the homogeneous, no-slip model with the transient model will provide insight into the effects of nonhomogeneous flow for the THTF transient test conditions.

Figure 17 shows the transient model reference case compared with the homogeneous model for the early transient portion of test 3.06.6B. Test 3.06.6B involved a relatively slow depressurization rate, and the observed transient peaks in mass flux for the two models appear to be in phase. The smoothed input for the transient model did not include the fine structure observed for the homogeneous model, and as a result, this fine structure is not seen in the transient model results. Differences of ~30 to 40% are observed from 0.5 to 2.0 s into the transient and near the mass

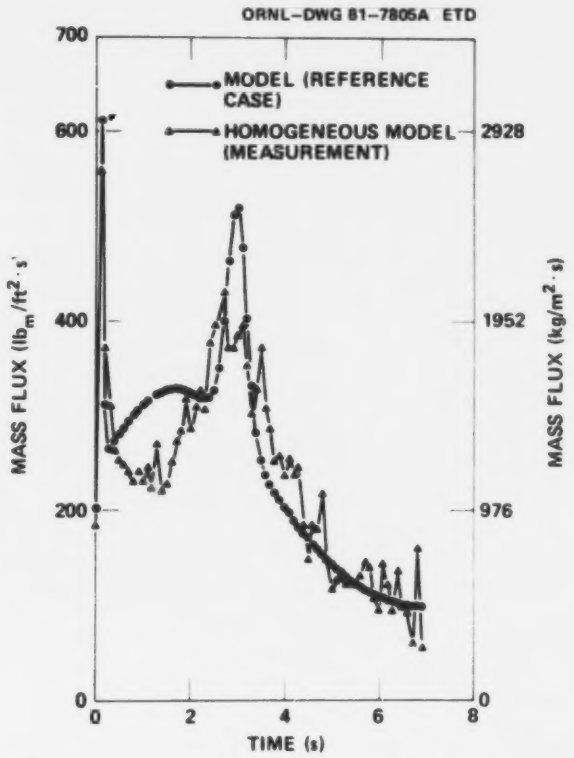

Fig. 17. Mass flux comparison between K & L reference-case model and homogeneous TBM-GAM3 model at B01 spool piece for test 3.06.6B.

BEST DOCUMENT AVAILABLE

flux peak seen at ~3 s. From 5 s to the end of the transient period shown, the fine structure of the homogeneous model varies around that of the transient model. Figure 18 shows the effect of varying the liquid-phase distribution coefficient for the same test. The effects are considerable for higher mass flux but negligible for mass flux below ~610 $kg/m^2 \cdot s$ (125 $lb_m/ft^2 \cdot s$), with the magnitude of the mass flux increasing with decreasing C_ℓ. Characterization of the appropriate value of C_ℓ is difficult, especially during the initial voiding of the test section, because flow regimes may vary considerably. Simple approximations for velocity and void profiles may yield values over the ranges indicated in Fig. 18. A simple model for an annular flow regime results in a value of 1.35 when substituted into Eq. (9). A stratified flow in horizontal spool pieces may produce a value of 0.7. Flow with flat profiles both in void fraction and velocity generates a C_ℓ of 1. Without experimental validation, values of C_ℓ obtained from simple models and applied to two-phase

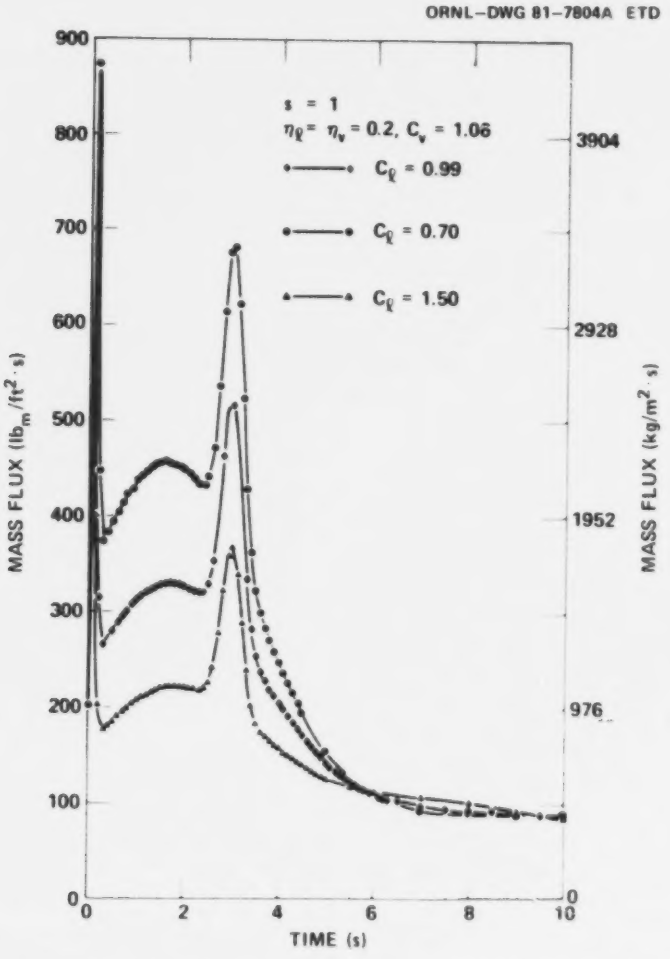

Fig. 18. Effect of the correlation coefficient C_ℓ on K & L model mass flux for test 3.06.6B.

BEST DOCUMENT AVAILABL

flow regimes where velocity and void profiles are varying in time as well as space may be misleading. Note that for test 3.06.6B, the important heat transfer data of interest are obtained from ~6 s to the end of the transient period shown. During this time, the effects of varying C_ℓ are negligible. Also during this period, the conditions in the upper test section bundle and outlet spool pieces were similar to those of the steady-state data discussed earlier.

The effect of varying the slip ratio in the transient K and L model is shown in Fig. 19. A pronounced effect is observed in the early portions of the transient and for higher mass fluxes. The effect is not as

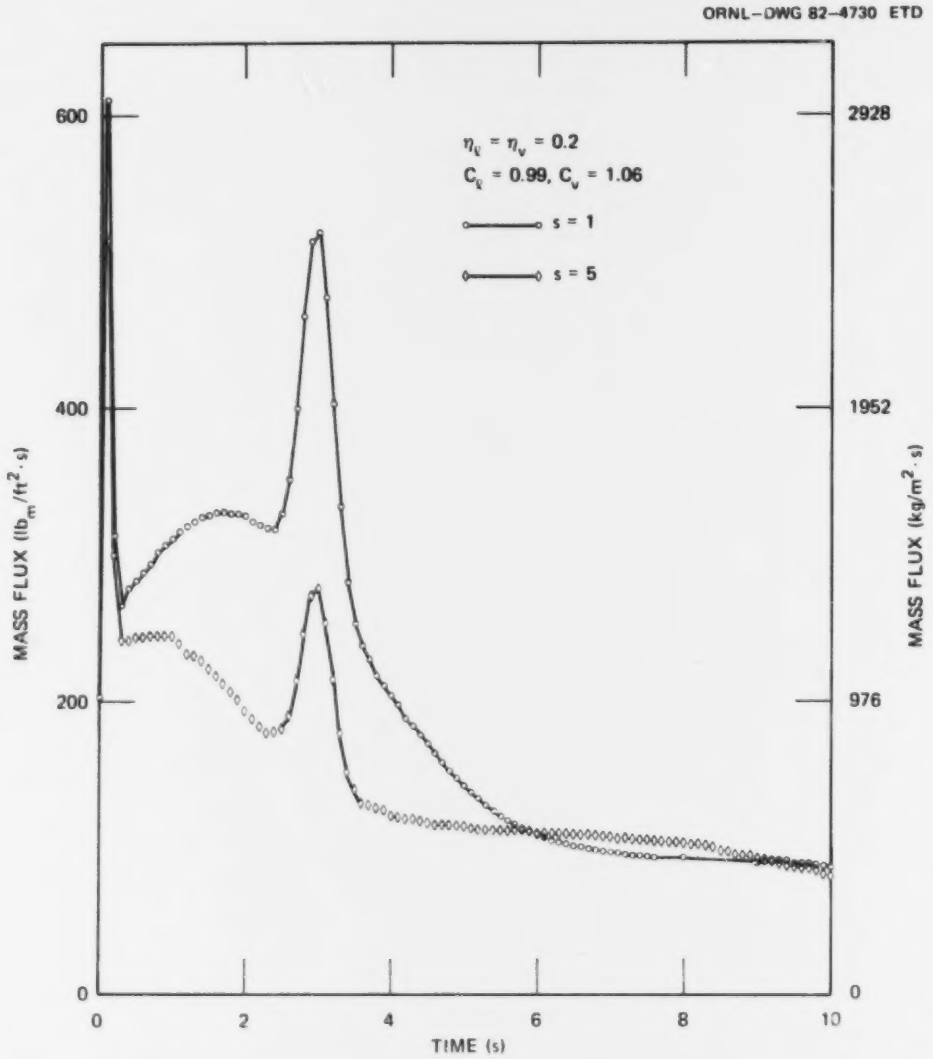

Fig. 19. Effect of slip on K & L mass flux model at B01 spool piece for test 3.06.6B.

BEST DOCUMENT AVAILABLE

great for times after ~6 s. For comparison, the K and L model was applied to the steady-state data discussed earlier by using various slip ratios. The results are shown in Figs. 20–22 as a function of inlet mass flux, pressure, and equilibrium quality. Variation of the slip ratio from 1.0 to 5.0 results in K and L model mass flux variation of ~10 to 15% over the steady-state test parameter ranges. Significant trends with pressure, mass flux, or equilibrium quality were not apparent. The mass flux ranges for the steady-state tests were in the range of the mass flux observed during the later transient periods of test 3.06.6B (>6 s).

The reference model case is compared with the homogeneous model for the faster transient of test 3.05.5B (Fig. 23). The reference model leads the homogeneous model by ~50 ms, presumably because of rotor inertia effects. The second peak agrees well temporally although the peak magnitude differs by ~25%. The two models do not agree very well for times shown after 1.25 s.

The effect of varying the liquid-phase distribution coefficient for test 3.05.5B is shown in Fig. 24. Significant differences (~40%) are observed as C_ℓ varies from the reference-case value of 0.99. The model using $C_\ell = 1.5$ interestingly reflects the increase in mass flux shown by the homogeneous model in Fig. 23 from ~3 to 4 s into the transient, whereas the cases with lower values of C_ℓ do not. In contrast to test 3.06.6B, considerable errors may result from uncertainties in C_ℓ even at low mass flux values for the conditions of test 3.05.5B.

Figure 25 shows the effect of varying the slip ratio for the transient model for test 3.05.5B. A change in slip ratio leads to a change in amplitude as well as temporal phase (i.e., the larger the slip ratio, the smaller the magnitude and the earlier the peak). The slip ratio of five is probably higher than would be expected under THTF test conditions, but the comparison shows the trends clearly.

An example of the relationship between the input data and the reference-case transient model output is shown in Fig. 26 for test 3.05.5B. The curves for pressure P, average mixture density D, and counting rate CR are smoothed analytical forms of discrete data measured during the test. The void fraction α and mass flux G are generated by the model. The mass flux and turbine meter counting rate are seen to be intimately related as the impulse and response. The effect of rotor inertia is observed in the second peak where the counting rate of the turbine meter lags the model predicted mass flux.

BEST DOCUMENT AVAILABLE

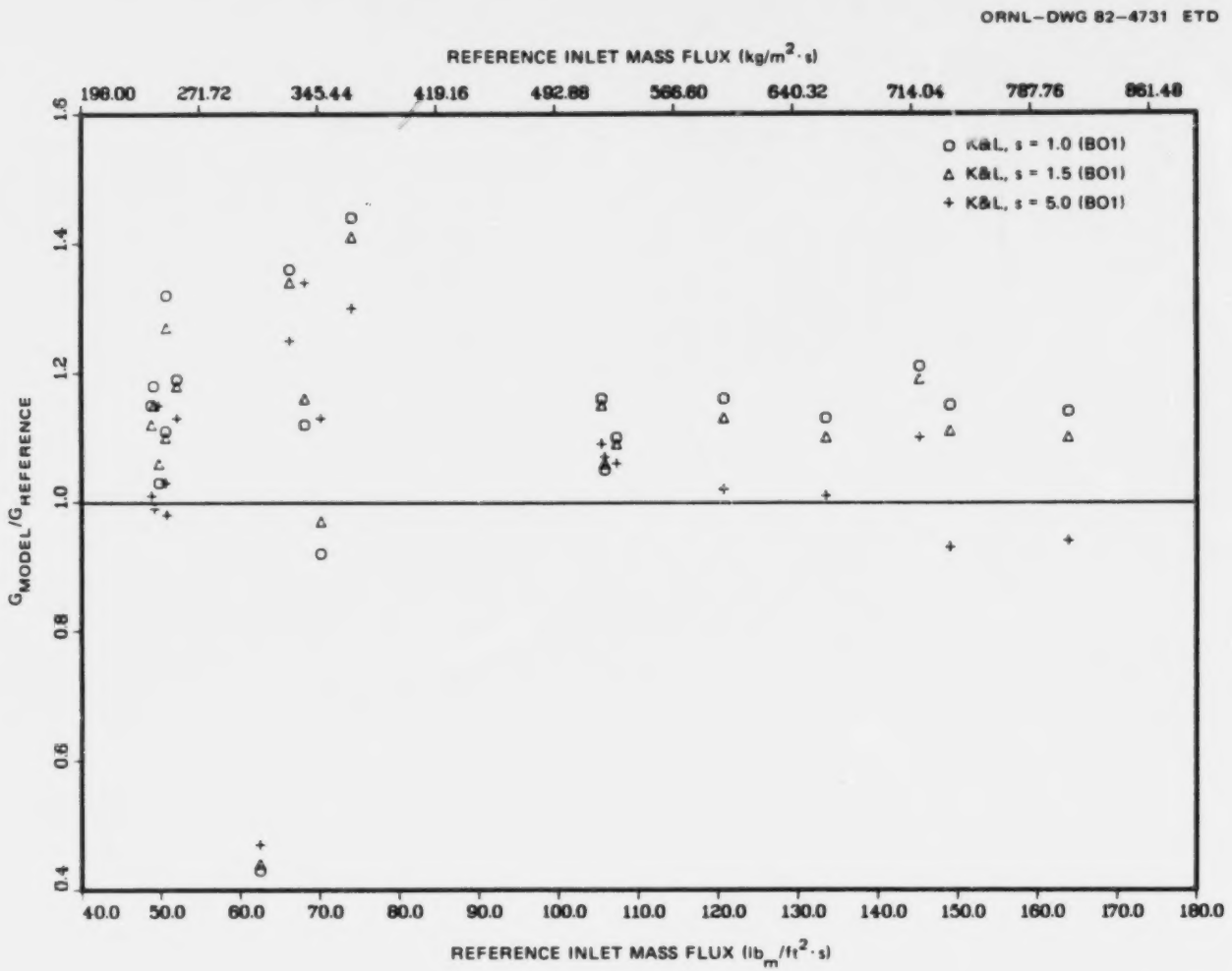

Fig. 20. Effect of slip on steady-state K & L mass flux model vs inlet mass flux at B01 spool piece.

BEST DOCUMENT AVAILABLE

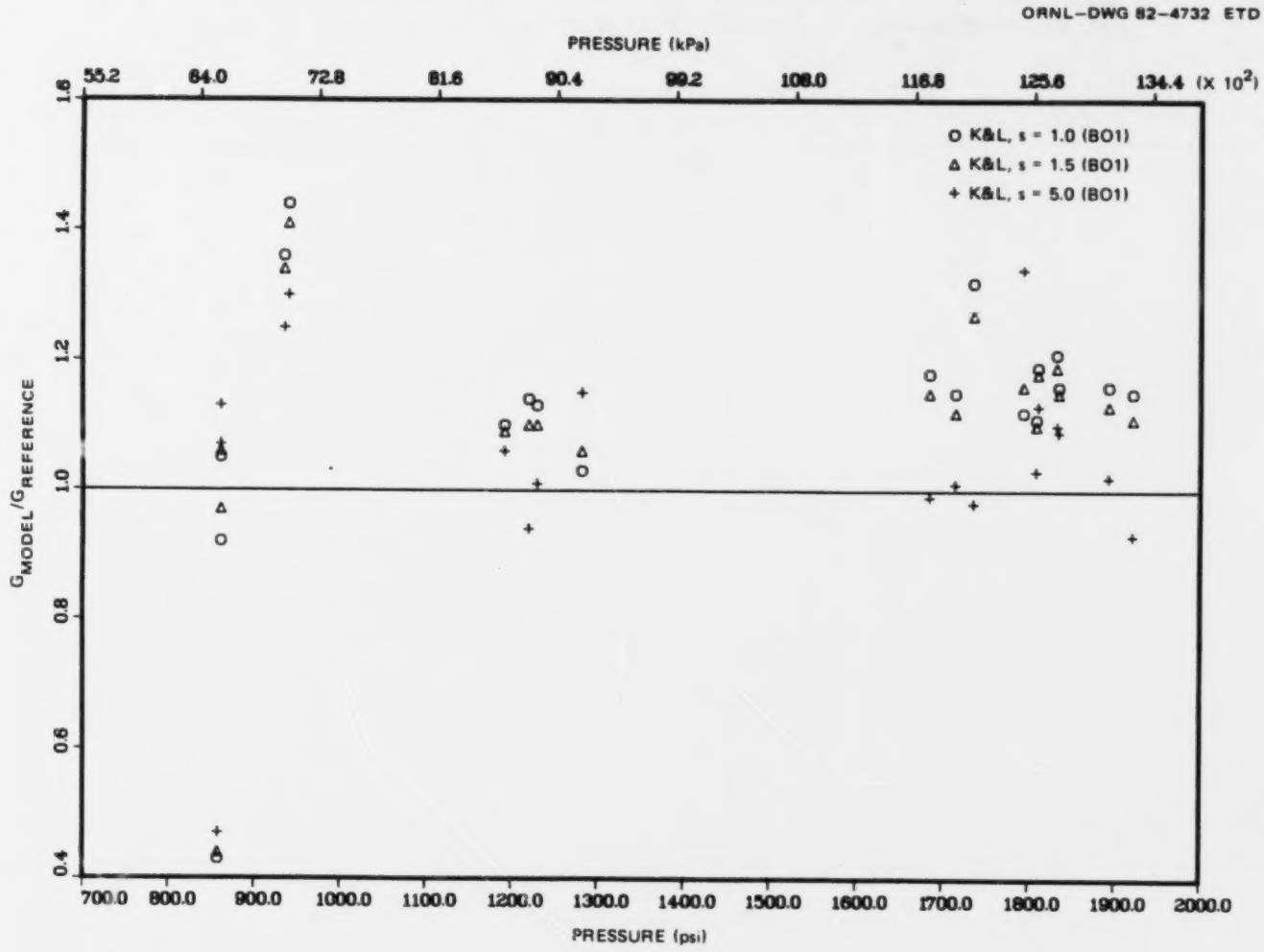

Fig. 21. Effect of slip on steady-state K & L mass flux model vs pressure at BO1 spool piece.

BEST DOCUMENT AVAILABLE

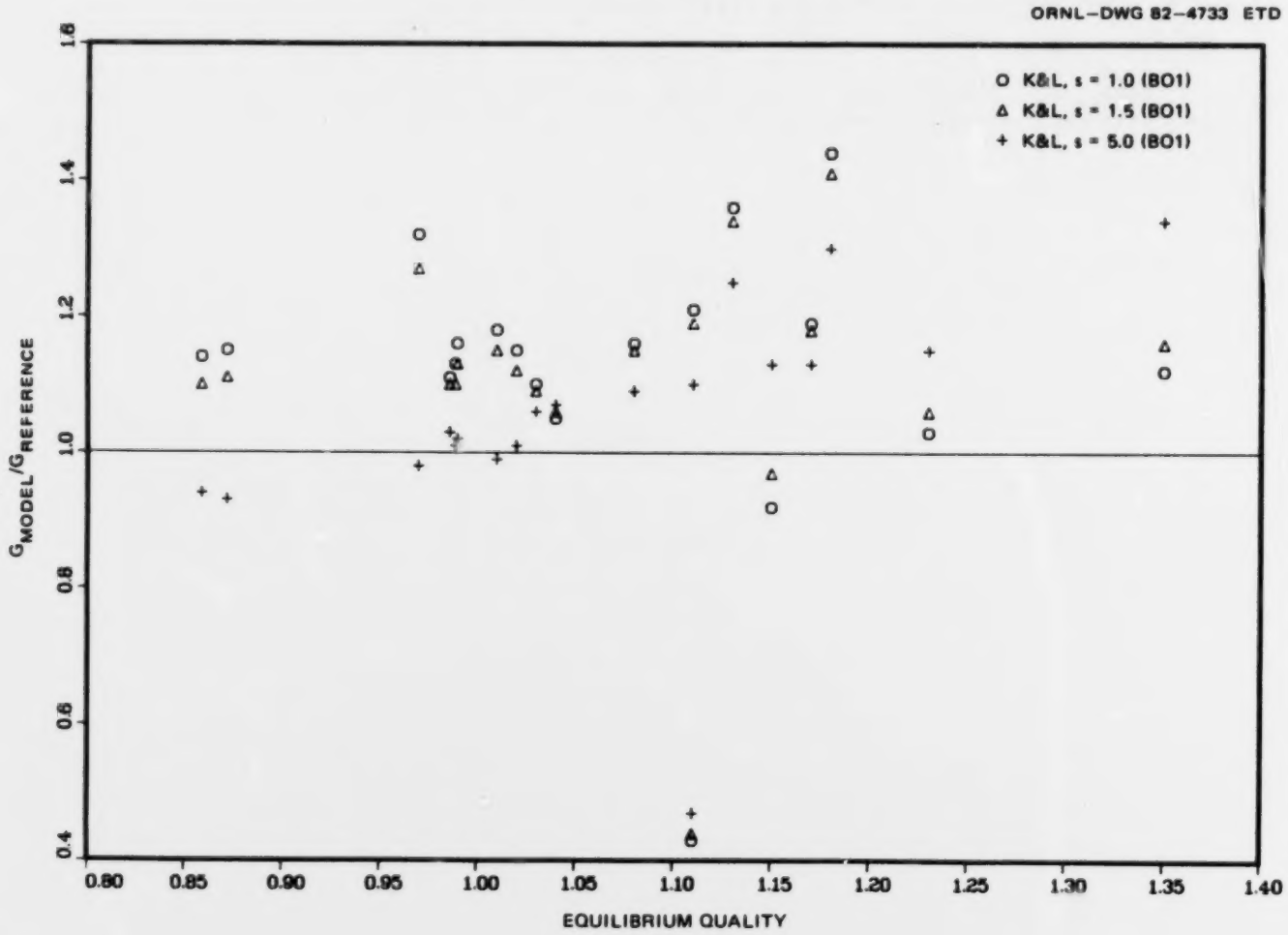

Fig. 22. Effect of slip on steady-state K & L mass flux model vs equilibrium quality at B01 spool piece.

BEST DOCUMENT AVAILABLE

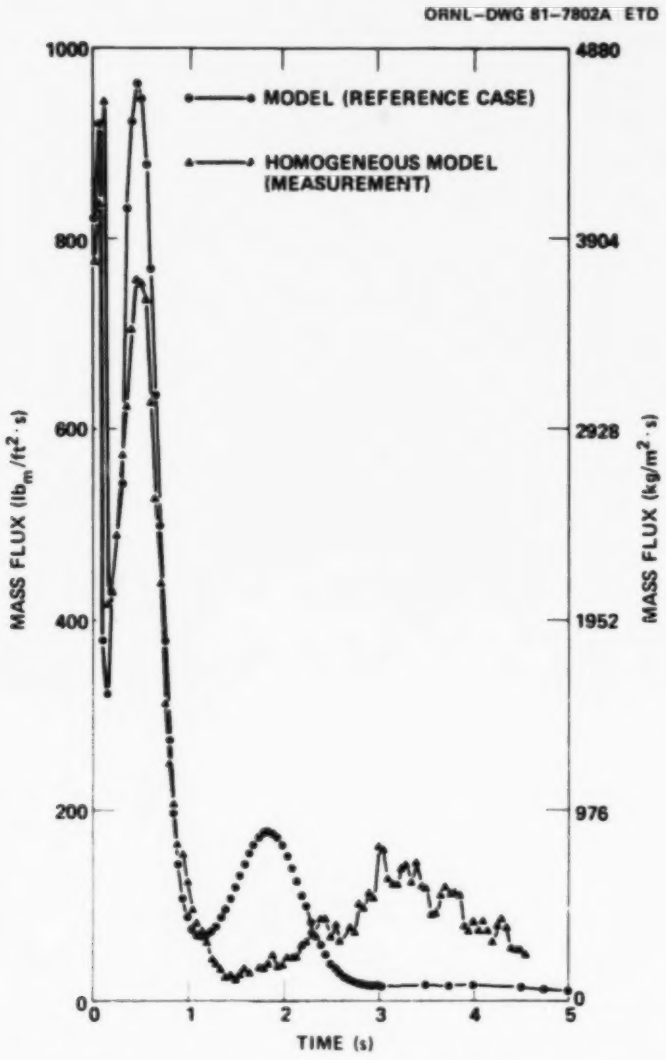

Fig. 23. Mass flux comparison between K & L reference-case model and homogeneous TBM-GAM3 model at B01 spool piece for test 3.05.5B.

BEST DOCUMENT AVAILABLE

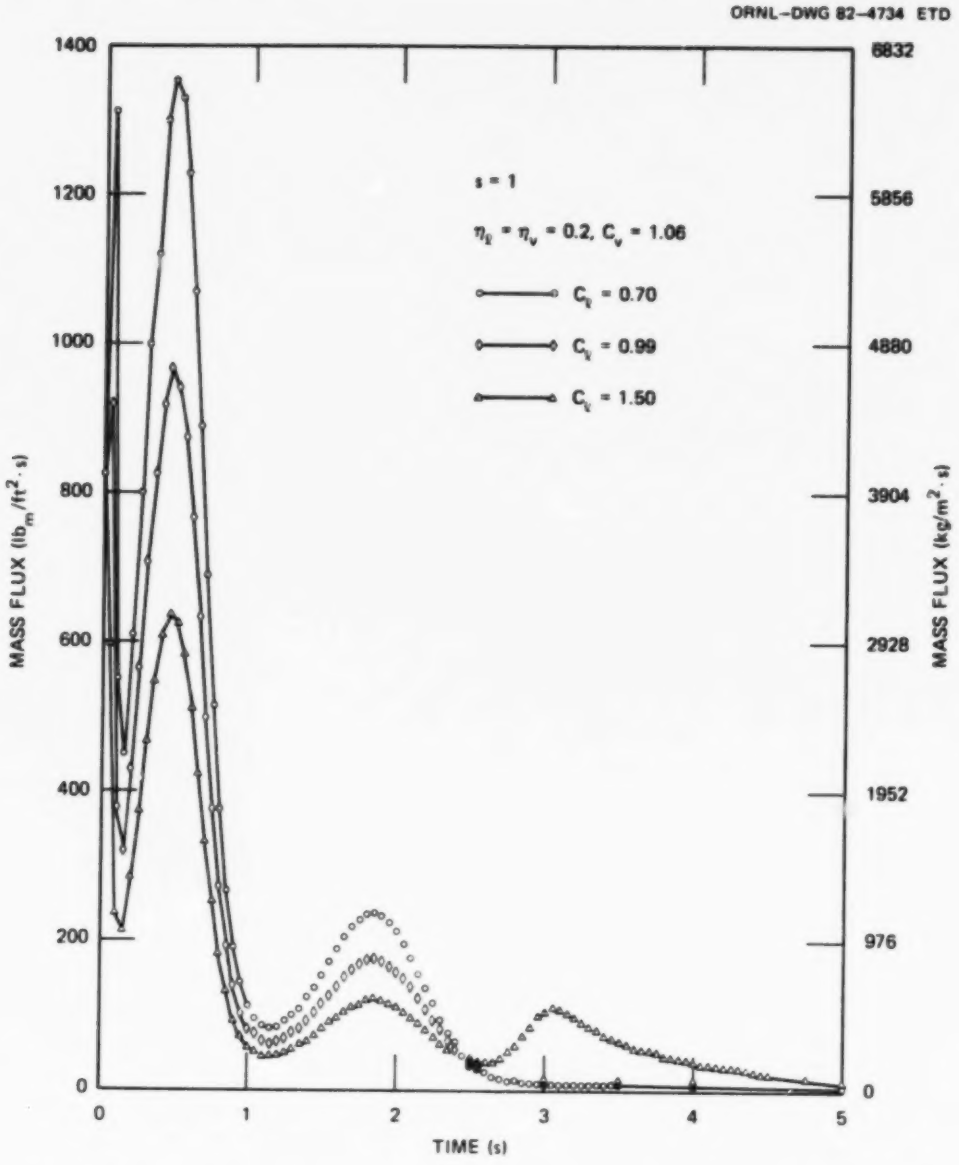

Fig. 24. Effect of correlation coefficient C_ℓ on K & L model mass flux for test 3.05.5B.

BEST DOCUMENT AVAILABLE

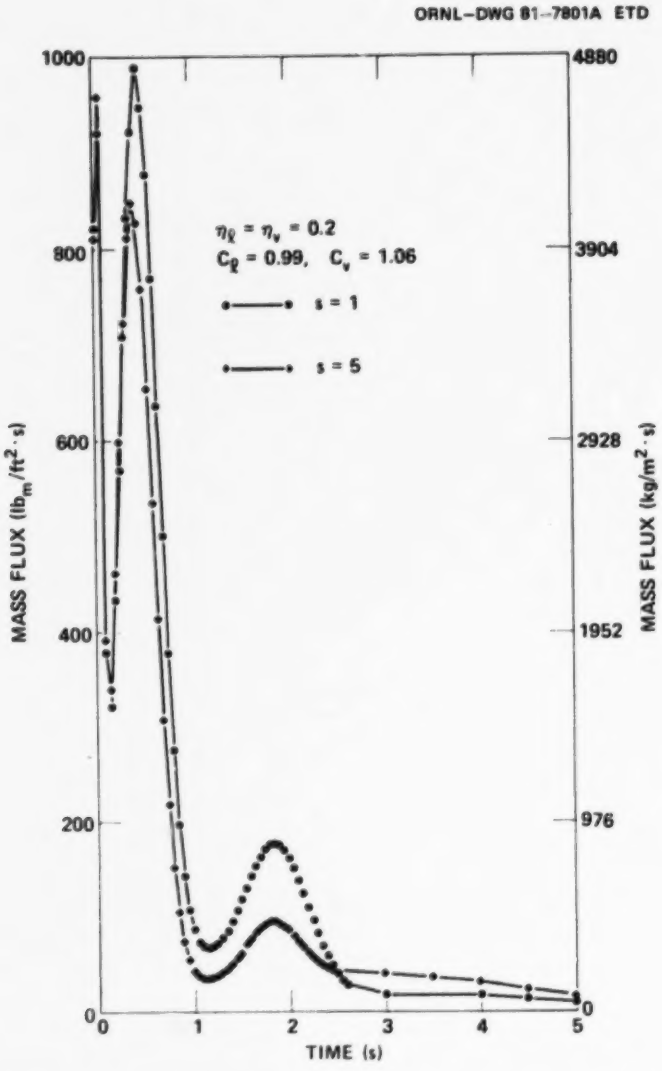

Fig. 25. Effect of slip on K & L mass flux model at B01 spool piece for test 3.05.5B.

BEST DOCUMENT AVAILABLE

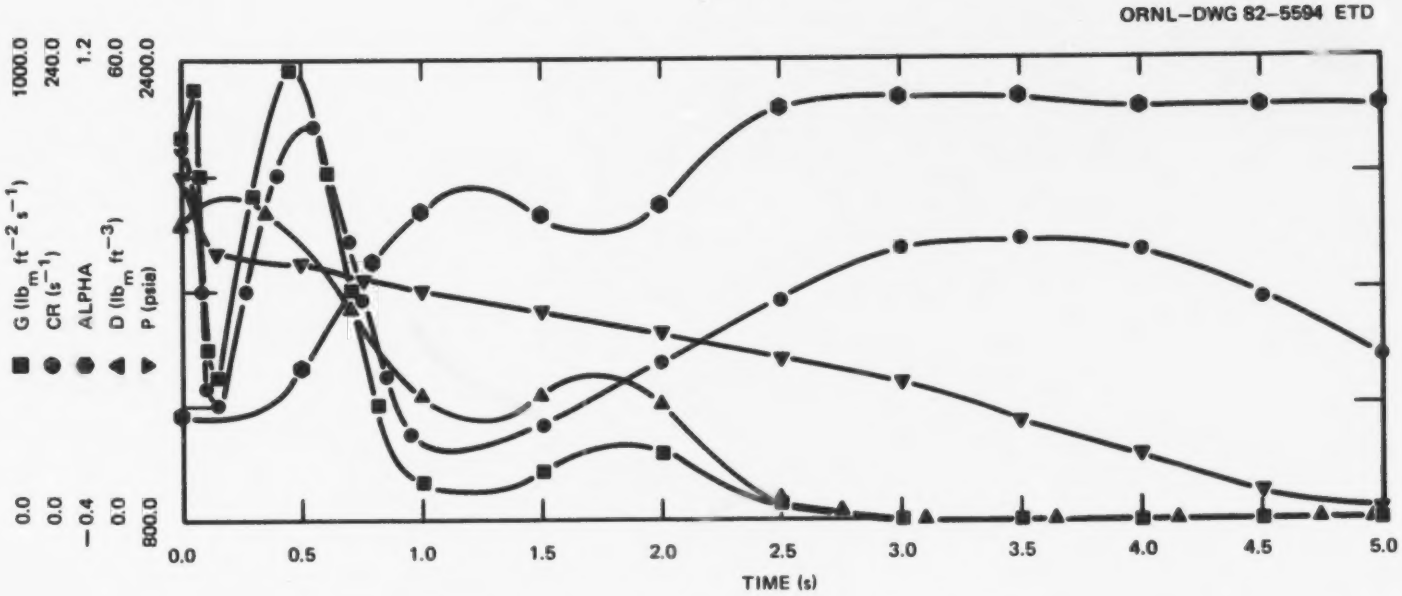

Fig. 26. Example of relationship between input and output parameters of transient K & L model for test 3.05.5B.

BEST DOCUMENT AVAILABLE

5. SUMMARY AND CONCLUSIONS

Steady-state tests indicate two-phase flow uncertainty bands of less than ±50% of reading (95% confidence bands) for all models at the B01 spool piece where a three-beam densitometer is used in applicable models. The DD-GAM3 and TBM-DD models actually show somewhat smaller uncertainty bands (±30%) than the TBM-GAM3 model at the Bundle Outlet spool piece (B01). However, at the Vertical Outlet spool piece (SVO), uncertainty bands for the DD-GAM model (70%) and the TBM-DD model (140%) are significantly higher. The sometimes large uncertainties in models that use measurements from the drag disks are not particularly surprising from the standpoint of previous operating experience. The drag disks are the least reliable of the spool-piece instruments in terms of repeatability and consistency of instrument response.

Significant uncertainty band increases result from using a single-beam densitometer as compared with using a three-beam densitometer. At the B01 spool piece for the turbine meter/densitometer model, the use of a single-beam densitometer results in an increase of uncertainty bands from ±50% (three-beam) to ±80% of reading. Similar results are observed for the drag disk/densitometer model where the use of a single-beam densitometer adds an additional 10% of reading to the uncertainty bands.

The application of a transient turbine meter model to transient THTF test data provides insight into possible transient uncertainties included in turbine meter/densitometer models. Comparison of the K and L transient model with the homogeneous model TBM-GAM3 indicates that the effects of the velocity profiles of the liquid phase, void profiles, rotor inertia, and slip are the most significant for the THTF transients of interest.

During the initial transient portion of the Upflow Film Boiling Test (3.06.6B) and for mass flux greater than ~610 $kg/m^2 \cdot s$ (125 $lb_m/ft^2 \cdot s$), variations in the transient model mass flux of 30 to 50% are observed as the void and velocity profile correlation coefficient C_ℓ is varied from 1.0 over a range of 0.7 to 1.5. For the same test, when mass flux is <610 $kg/m^2 \cdot s$ (the time period where film boiling heat transfer data of interest are available), the effect of varying C_ℓ is negligible. In contrast to test 3.06.6B, considerable errors may result from uncertainties in C_ℓ even at low mass flux values for the conditions of test 3.05.5B.

Increases in slip from 1.0 reduce the magnitude of the model mass flux and slow time response of the turbine meter. The effect of slip is significant for both tests during the early fast transient periods. For test 3.06.6B, the effect is not as great for times after ~6 s. The application of the K and L steady-state model to the steady-state data indicates variations of ~10 to 15% as the slip ratio varies from 1 to 5. The high-quality two-phase flow conditions of the later transient periods of test 3.06.6B are expected to be similar to those of the steady-state tests.

Rotor inertia effects are significant for fast transients such as the early portions of the Double-Ended Cold Leg Break Test (3.05.5B). The reference-case transient model leads the homogeneous model by ~50 ms during portions of the transient, resulting in significant mass flux differences. Response time effects were not as significant for the slower transients of

BEST DOCUMENT AVAILABLE

the Upflow Film Boiling Test (3.06.6B), although mass flux differences of 30 to 40% between the transient model reference case and the homogeneous model are observed.

Because the actual mass flux is not known for the transient cases, neither model may be verified. The model comparisons are able to provide test specific information on mass flux sensitivity to uncertainties in two-phase flow parameters.

The K and L model results agreed well with the TBM-GAM3 model for the Steady-State Upflow Film Boiling Test data. For this reason and lacking any additional information, to estimate uncertainties during the faster transient portions of the THTF tests, the addition of the steady-state uncertainty estimates and the transient uncertainty estimates based on transient model comparisons to obtain a total transient uncertainty estimate would appear to be warranted. Note that in terms of heat transfer data, the mass flux is changing fairly slowly during the important periods of interest for the transient Upflow Film Boiling Tests. Additionally, the outlet flow conditions of the Steady-State Upflow Film Boiling Tests were similar to the higher quality portions of the transient tests. Application of the steady-state uncertainty bands over these conditions can be made with a good degree of confidence.

Although the steady-state uncertainty data provides a good estimate of uncertainty bands over the flow conditions and parameter ranges observed for those steady-state tests, uncertainties for different quality ranges and flow regimes may be considerably different. Without data over other ranges, however, these are the best available uncertainty estimates for use in two-phase flow conditions at the THTF.

BEST DOCUMENT AVAILABLE

REFERENCES

1. P. S. Kamath and R. T. Lahey, *A Turbine Meter Evaluation Model for Two Phase Transients*, Rensselaer Polytechnic Institute, NES-459 (October 1977).

2. K. G. Turnage, *Two-Phase Flow Measurements with Advanced Instrumented Spool Pieces*, NUREG/CR-1529 (ORNL/NUREG-72) (September 1980).

3. C. B. Mullins et al., *Thermal-Hydraulic Test Facility Experimental Data Report for Test 3.06.6B – Transient Film Boiling in Upflow*, ORNL/NUREG/TM-407, Vol. 3 (to be published).

4. C. B. Mullins et al., *Thermal-Hydraulic Test Facility Experimental Data Report for Test 3.03.6AR – Transient Film Boiling in Upflow*, ORNL/NUREG/TM-407, Vol. 2 (to be published).

5. C. B. Mullins et al., *Thermal-Hydraulic Test Facility Experimental Data Report for Test 3.08.6C – Transient Film Boiling in Upflow*, ORNL/NUREG/TM-407, Vol. 4 (to be published).

6. C. B. Mullins et al., *Thermal-Hydraulic Test Facility Experimental Data Report for Test 3.05.5B Transient Film Boiling in Upflow*, ORNL/NUREG/TM-407, Vol. 5 (to be published).

7. D. K. Felde et al., *Facility Description – Thermal Hydraulic Test Facility (THTF) MOD3, ORNL Blowdown Heat Transfer Program*, ORNL/TM-7842 (to be published).

8. K. G. Turnage, C. E. Davis, and D. G. Thomas, *Advanced Two-Phase Flow Instrumentation Program Quart. Prog. Rep. for July–September 1978*, NUREG/CR-0686 (ORNL/NUREG/TM-309).

9. K. G. Turnage and P. A. Jallouk, *Advanced Two-Phase Instrumentation Program Quart. Prog. Rep. for April–June 1978*, NUREG/CR-0501 (ORNL/NUREG/TM-279).

10. J. Teague, II, *AMICON – A Multi-Model Interpretive Code for Two Phase Flow Instrumentation with Uncertainty Analysis*, K/CSD/TM-38 (to be published).

11. IBM, *Continuous System Modeling Program III (CSMP III) Program Reference Manual*, SH19-7001-3 (December 1975).

12. S. Rouhani, "Application of the Turbine Type Flow Meters in the Measurement of Steam Quality and Void," presented at the Symposium on In-Core Instrumentation, Oslo, Norway, June 15, 1964.

BEST DOCUMENT AVAILABLE

BLANK PAGE

NUREG/CR-2544
ORNL/TM-7859
Dist. Category AN

Internal Distribution

1. T. M. Anklam
2-6. N. C. J. Chen
7. S. K. Combs
8-9. W. G. Craddick
10-14. D. K. Felde
15. T. J. Hanratty (Consultant)
16. J. E. Hardy
17. H. W. Hoffman
18. A. L. Lotts
19. D. G. Morris
20. C. B. Mullins
21. R. W. Murphy
22. L. J. Ott
23. T. W. Robinson, Jr.
24. D. G. Thomas
25. H. E. Trammell
26. D. B. Trauger
27. J. D. White
28. G. L. Yoder
29. ORNL Patent Office
30. Central Research Library
31. Document Reference Section
32-33. Laboratory Records Department
34. Laboratory Records (RC)

External Distribution

35-36. Director of Division of Reactor Safety Research, Nuclear Regulatory Commission, Washington, DC 20555
37. Director, Reactor Division, DOE, ORO, Oak Ridge, TN 37830
38. Office of Assistant Manager for Energy Research and Development, DOE, ORO, Oak Ridge, TN 37830
39-43. Director, Reactor Safety Research Coordination Office, DOE, Washington, DC 20555
44-45. Technical Information Center, DOE, Oak Ridge, TN 37830
46-145. Give distribution as shown under category AN (NTIS-10)

BEST DOCUMENT AVAILABLE